N86-30172

BACKWARD WHIRL IN A SIMPLE ROTOR SUPPORTED ON HYDRODYNAMIC BEARINGS

R. Subbiah, R.B. Bhat, and T.S. Sankar
Concordia University
Montreal, Canada

J.S. Rao
Indian Embassy
Washington, D.C.

The asymmetric nature of the fluid film stiffness and damping properties in rotors supported on fluid film bearings causes a forward or a backward whirl depending on the bearing parameters and the speed of the rotor. A rotor was designed to exhibit backward synchronous whirl. The rotor-bearing system exhibited split criticals, and a backward whirl was observed between the split criticals. The orbital diagrams show the whirl pattern.

INTRODUCTION

The design of a rotor system must consider several aspects such as critical speeds, peak unbalance response, regions of change of whirl directions, and instability. In general, large rotor systems in continuous operation are supported on hydrodynamic bearings. These hydrodynamic bearings exhibit asymmetric cross-coupled stiffness and damping properties that vary with the speed of operation. Such a property influences the dynamic behavior of the rotors significantly.

The dynamic behavior of such rotors can be predicted by using transfer matrix methods, finite elements, modal analysis, etc. [1-6]. Rao [7] and Rao et al. [8] used a simple analytical technique to predict the dynamic behavior of such rotors. They studied a single-disk rotor on fluid film bearings and observed that for specific rotor-bearing parameter combinations the system may exhibit two distinct peaks in the response but sometimes it may show only one peak in the response. Kollmann and Glienicke [9] have shown experimentally the existence of the split criticals in a simple rotor supported on fluid films bearings. Kellenberger [10] derived equations for double frequency accelerations in turbogenerator rotors resulting from anisotropy in the plain cylindrical bearings and showed the occurrence of backward whirl between the criticals. These studies predict a forward whirl before the first critical and after the second critical, whereas the rotor executes a backward whirl between the two criticals. Also, the simple rotor with only a single peak in its response is known to whirl in the forward direction at all speeds.

Several experimental investigations are reported in the literature regarding the dynamic behavior of different types of rotor systems supported on hydrodynamic bearings. A few notable works are by Yamamoto [11], Hull [12], and Lund and Orcutt [13].

Most of the referred work on practical rotors supported on hydrodynamic bearings does not satisfy conditions for a clear backward whirl and hence the phenomenon of backward whirl has so far not been observed experimentally. The occurrence of backward whirl is also not desirable in practice. In the present work conditions are derived for backward whirl considering bearing damping. Further results of the

experiments carried out on a laboratory rotor model designed so as to exhibit backward whirl are reported.

NOMENCLATURE

a	disk eccentricity
c	shaft damping
$c_{zz}, c_{yy}, c_{yz}, c_{zy}$	fluid film damping coefficients
$E_i, \bar{E}_i$	forward and backward component, respectively, of i^{th} modal force vector
F	overall exciting force vector
K	overall stiffness matrix
k	shaft stiffness
$k_{zz}, k_{yy}, k_{yz}, k_{zy}$	fluid film stiffness coefficients
M	overall mass matrix
$N_i, \bar{N}_i$	forward and backward component of i^{th} modal displacement vector
q	displacement vector at disk location
q_j	displacement vector at bearing location
r	maximum unbalance response of rotor
z, y	displacement of rotor at disk location in Z and Y directions
z_0, y_0	displacement of rotor at bearing location in Z and Y directions
η_i	i^{th} modal displacement vector
λ_i	i^{th} complex eigenvalue
φ	right eigenvector of system
φ^*	left eigenvector of system

ANALYSIS

A schematic of the rotor is shown in Fig. 1. Equations of motion of the rotor are

$$m \frac{d^2}{dt^2} (z + a \cos \omega t) + k(z - z_0) + c(\dot{z} - \dot{z}_0) = 0 \qquad (1a)$$

$$m\dot{z} - m\dot{z} = 0 \qquad (1b)$$

$$m\ddot{y} - \dot{m}\dot{y} = 0 \tag{1c}$$

$$m\frac{d^2}{dt^2}(y + a \sin \omega t) + k(y - y_0) + c(\dot{y} - \dot{y}_0) = 0 \tag{2}$$

and the constraint equations are

$$k(z - z_0) + c(\dot{z} - \dot{z}_0) = 2k_{zz} \cdot z_0 + 2c_{zz} \cdot \dot{z}_0 + 2k_{zy} \cdot y_0 + 2c_{zy} \cdot \dot{y}_0 \tag{3}$$

$$k(y - y_0) + c(\dot{y} - \dot{y}_0) = 2k_{yy} \cdot y_0 + 2c_{yy} \cdot \dot{y}_0 + 2k_{yz} \cdot z_0 + 2c_{yz} \cdot \dot{z}_0 \tag{4}$$

Equations (1) to (4) can be written in the form

$$[M]\{\dot{Q}\} + [K]\{Q\} = \{F\} \tag{5}$$

where

$$[M] = \begin{bmatrix} \ddot{z} & \ddot{y} & \dot{z} & \dot{y} & \dot{z}_0 & \dot{z}_0 \\ 0 & 0 & m & 0 & 0 & 0 \\ 0 & 0 & 0 & m & 0 & 0 \\ m & 0 & c & 0 & -c & 0 \\ 0 & m & 0 & c & 0 & -c \\ 0 & 0 & c & 0 & -(c+2c_{zz}) & -2c_{zy} \\ 0 & 0 & 0 & c & -2c_{yz} & -(c+2c_{yy}) \end{bmatrix}$$

$$[K] = \begin{bmatrix} \dot{z} & \dot{y} & z & y & z_0 & y_0 \\ -m & 0 & 0 & 0 & 0 & 0 \\ 0 & -m & 0 & 0 & 0 & 0 \\ 0 & 0 & k & 0 & -k & 0 \\ 0 & 0 & 0 & k & 0 & -k \\ 0 & 0 & k & 0 & -(k+2k_{zz}) & -2k_{zy} \\ 0 & 0 & 0 & k & -2k_{yz} & -(k+2k_{yy}) \end{bmatrix}$$

$$\{Q\} = \begin{bmatrix} \dot{z}, & \dot{y}, & z, & y, & z_0, & y_0 \end{bmatrix}^T$$

$$\{F\} = [0,\ 0,\ ma\omega^2 \cos \omega t,\ ma\omega^2 \sin \omega t,\ 0,\ 0]$$

The eigenvalues and eigenvectors of the system are obtained by solving the homogeneous form of equations (6) as shown below:

$$[M]\{\dot{Q}(t)\} + [K]\{Q(t)\} = 0 \tag{6}$$

Assuming a solution of the form

$$\{Q(t)\} = \{\varphi\} \exp(\lambda t) \tag{7}$$

where $\{\varphi\}$ represent the system eigenvectors, and substituting equation (7) in equation (8) the eigenvalue problem becomes

$$\lambda[M]\{\varphi\} + [K]\{\varphi\} = 0 \tag{8}$$

Because of the presence of asymmetric cross-coupled stiffness and damping coefficients in the bearings, the matrices [M] and [K] are nonsymmetric, resulting in a non-self-adjoint system. Hence a conventional normal-mode method is not possible, and it is essential to consider that the biorthogonality property of the modes of the original system are those of the transposed system to the uncoupled equations of motion. THe left eigenvectors are obtained by transposing matrices [M] and [K] in equation (6). The eigenvalues of the original and transposed systems are identical, but the eigenvectors are different.

The solution of equation (5) is assumed in the form

$$\{Q(t)\} = [\varphi]\{\eta(t)\} \tag{9}$$

where $[\varphi]$ contains the eigenvectors of the original system (which are called right eigenvectors). Introducing equation (9) in equation (5) and premultiplying the result by $[\varphi^*]^T$, which is the left eigenvector of the system, lead to the following uncoupled equations:

$$[\mu]\{\ddot{\eta}(t)\} + [\kappa]\{\eta(t)\} = \{\sigma\} \tag{10}$$

where

$$[\mu] = [\varphi^*]^T[M][\varphi]$$

$$[\kappa] = [\varphi^*]^T[K][\varphi]$$

and

$$\{\sigma\} = [\varphi^*]^T\{F\}$$

Equation (10) results in uncoupled equation of the form

$$\mu_i\ddot{\eta}_i(t) + \kappa_i\eta_i(t) = \sigma_i(t) \tag{11}$$

This is solved by assuming steady-state solution of the form

$$\eta_i(t) = N_i \exp(j\omega t) + \bar{N}_i \exp(-j\omega t) \tag{12}$$

and

$$\sigma_i(t) = E_i \exp(j\omega t) + \bar{E}_i \exp(-j\omega t)$$

Substituting equation (12) in equation (11) results in

$$(\kappa_j + j\omega\mu_j)\, N_j \exp(j\omega t) + (\kappa_j - j\omega\mu_j)\, \bar{N}_j \exp(-j\omega t) = E_j \exp(j\omega t) + \bar{E}_j \exp(-j\omega t) \qquad (13)$$

Equating the coefficients of the forward and backward rotation terms, we obtain

$$N_j = \frac{\bar{E}_j}{k_j + j\omega\mu_j} \qquad (14)$$

$$\bar{N}_j = \frac{\bar{E}_j}{k_j - j\omega\mu_j}$$

Hence the displacements are determined from equations (10) to (14) and then the unbalance response of the rotor is obtained nondimensionally as

$$r = \frac{z + jy}{a} \qquad (15)$$

where a is the disk eccentricity. The complex eigenvalues are obtained from equation (6).

Depending on the bearing parameters the rotor will have either split criticals or just a single peak in the fundamental critical speed region, corresponding to synchronous whirl. In the case of the split criticals in the synchronous whirl, the backward component $\bar{N}_j$ is larger than the forward component N_j between the split criticals.

EXPERIMENTAL RESULTS

The details of the test rotor are given in table 1. It consists of a circular shaft with a circular disc at the center and supported on two identical hydrodynamic bearings at the ends. These bearings are mounted on cast iron pedestals at the two ends, and in turn these pedestals are rigidly fastened to the support, which is made of steel angles. The pedestals were impact excited both in the horizontal and vertical directions, and the resulting acoustical response was measured close to the pedestals. A frequency analysis of the measured sound showed that the first peak occurred at a much higher frequency than the critical speeds of the rotor, indicating that the pedestals were rigid. The bearings are supplied with oil through a gravity feed. The unbalance response of the shaft is measured in both the x and y directions by two proximity pickups. The signals from the pickups are fed to a twin-channel FFT analyzer, and the orbit diagrams are obtained with a x-y plotter. The direction of plotter pen motion indicated the direction of rotor whirl.

In designing the rotor such that it exhibits a backward whirl, the bearing coefficients to be used in equations (3) and (4) were taken from the results of Lund [14]. These results can also be found in [15]. Lund's results agree well with the experimentally determined bearing coefficients by Glienicke [9].

The whirl orbits obtained experimentally are shown normalized with respect to the disc eccentricity in Figs. 2 to 4 for different rotor speeds. Orbital diagrams are shown for a bearing clearance of 1.8796×10^{-4} m, since a backward whirl could be identified only for this case. The two critical speeds are 2200 and 2600 rpm. The rotation of the rotor is in the counterclockwise direction and hence Figs. 2 and 4 show forward whirls and Fig. 3 shows backward whirl. The speed corresponding to the backward whirl in Fig. 3 is 2500 rpm, which falls between the two criticals at 2200 and 2600 rpm. Since the backward whirl between the criticals is of interest, a photograph of backward whirl motion of the rotor at 2500 rpm was taken from the FFT analyzer screen. Theory also predicts these whirl directions, and hence there is a qualitative agreement between theory and experiments.

REFERENCES

1. Lund, J.W., 1965, Mechanical Technology Inc., Latham, N.Y., U.S.A., AFAPL-Tr-65-45, "Rotor Bearing Dynamics Design Technology, Part V: Computer Program Manual for Rotor Response and Stability".

2. Kramer, E., 1977, ASME Publication 77-DET-13, "Computation of Unbalance Vibrations of Turborotors".

3. Nelson, H.D. and McVaugh, J.N., 1976, Journal of Engineering for Industry, ASME, Vol. 98, p. 593, "The Dynamics of Rotor Bearing Systems Using Finite Elements".

4. Lalanne, M. and Queau, J.P., 1979, Societe Nationale des Industries Aerospatiales, "Calcul par Elements Finis du Comportement Dynamique des Chaines Cinematiques de Reducteur".

5. Morton, P.G., 1967-68, Proc. Inst. Mech. Engrs., Vol. 182, Part 1, No. 13, "Influence of Coupled Asymmetric Bearings on the Motion of a Massive Flexible Rotor".

6. Gunter, E.., Choy, K.C. and Allaire, P.E., "Modal Analysis of Turborotors using Planar Modes - Theory", Journal of the Franklin Institute, Vol. 305, No. 4, April 1978.

7. Rao, J.S., 1982, Mechanism and Machine Theory Journal, Vol. 17, No. 2, "Conditions for Backward Synchronous Whirl of a Flexible Rotor in Hydrodynamic Bearings".

8. Rao, J.S., Bhat, R.B. and Sankar, T.S., 1980-81, Transactions of the Canadian Society of Mechanical Engineers, Vol. 6, No. 3, pp. 155-161, "A Theoretical Study of the Effect of Damping on the Synchronous Whirl of a Rotor in Hydro-Dynamic Bearings".

9. Kollmann, K. and Glienicke, J., JSME, 1967, Semi-International Symposium 4th-8th Sept. 1967, Tokyo, "The behaviour of turbine bearings with respect to instability prediction".

10. Kellenberger, W., Proceedings of the Institution of Mechanical Engineers (London), 1980, Paper No. C312/80, P.415-520, "Double frequency

accelerations in turbogenerator rotors resulting from anisotrophy in the bearings".

11. Yamamoto, 1954, Memoirs of the Faculty of Engineering, Nagoya University Vol. 6, No. 2, p. 755, "On the Critical Speeds of a Shaft".

12. Hull, E.H., 1961, Journal of Engineering for Industry, Vol. 83, p. 219, "Shaft Whirling as Influenced by Stiffness Asymmetry".

13. Lund J.W. and Orcutt, F.K., 1967, Transactions of ASME, Journal of Engineering for Industry, Vol. 89, No. 4, "Calculations and Experiments on the Unbalance Response of a Flexible Rotor".

14. Lund, J.W., 1965, Mechanical Technology, Inc., AFAPL-Tr-65-45, "Rotor Bearings Dynamic Design Technology, Part III: Design Handbook for Fluid Bearings".

15. Rao, J.S., 1983, Wiley Eastern Limited, New Delhi, Rotor Dynamics.

TABLE 1: DETAILS OF TEST ROTOR

Shaft Diameter	0.0222 m
Shaft Length	0.5080 m
Weight of Disk	89 N
Shaft Stiffness	8.9×10^5 N/m
Bearing Diameter	0.0254 m
Bearing L/D Ratio	1
Oil Viscosity at 25.5°C	0.96×10^{-5} Pascal sec.
Unbalance of Rotor	1.084×10^{-4} kg.m
Bearing Clearance	1.8796×10^{-4} m (0.0074 in)

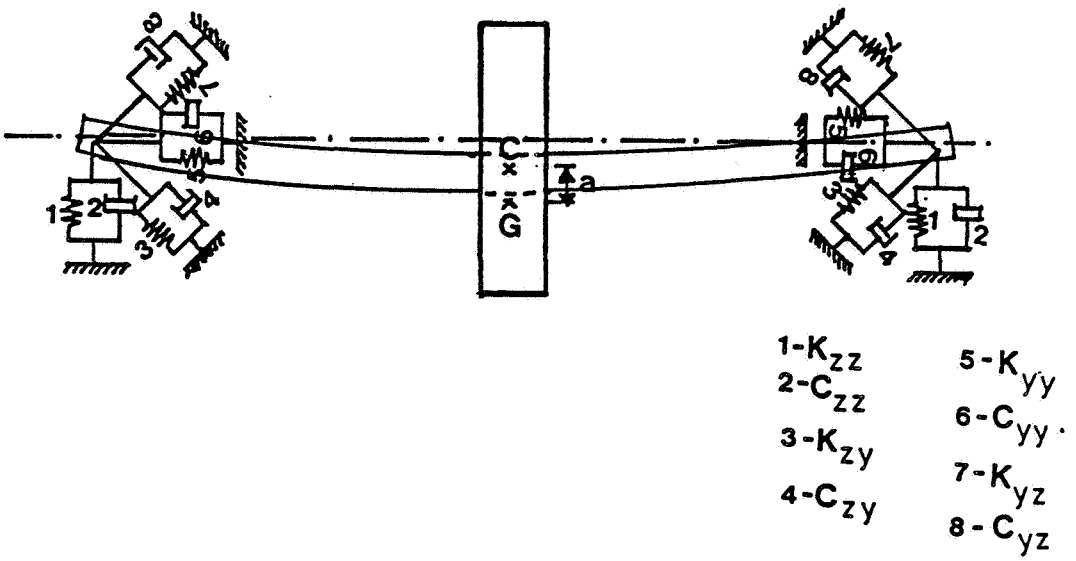

Figure 1. - Schematic diagram of single mass rotor.

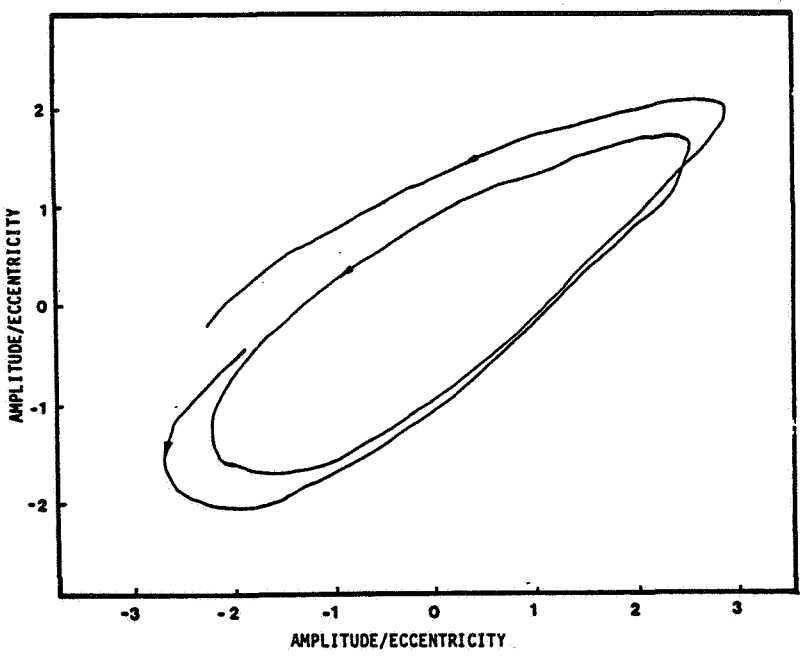

Figure 2. - Rotor whirl orbit at 2150 rpm (counterclockwise direction corresponds to forward whirl).

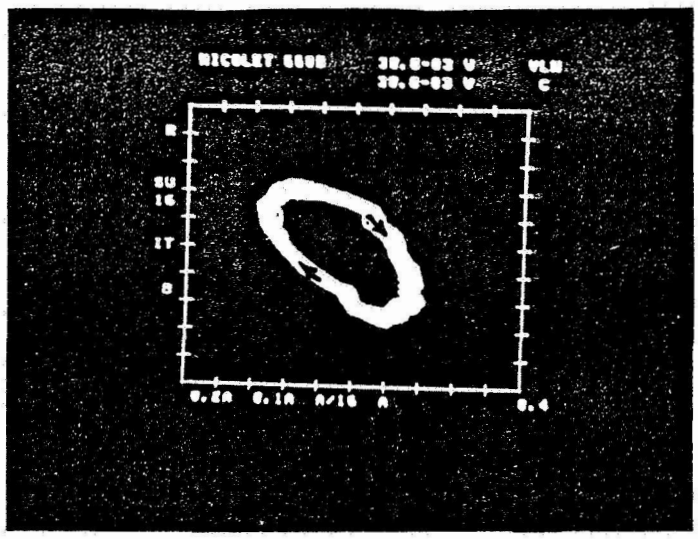

Figure 3. - Rotor whirl orbit at 2500 rpm (clockwise direction corresponds to backward whirl).

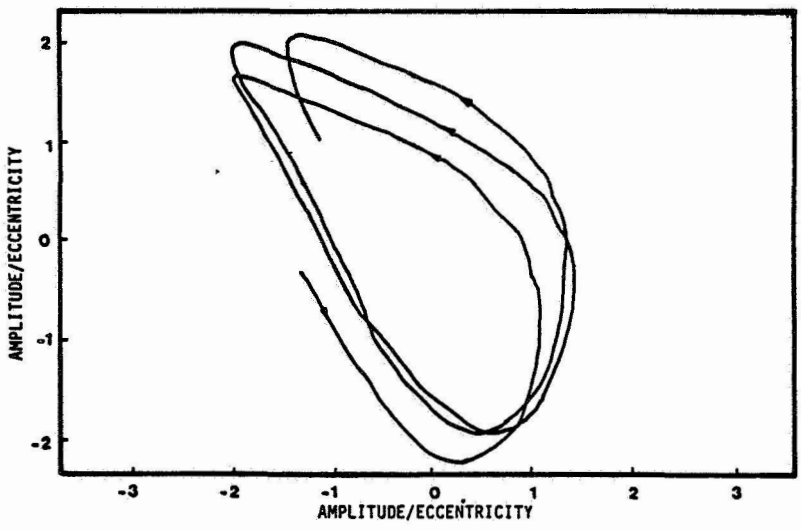

Figure 4. - Rotor whirl orbit at 3000 rpm (counterclockwise direction corresponds to forward whirl).